

PULSE INTENSITY MODULATION AND THE TIMING STABILITY OF MILLISECOND PULSARS: A CASE STUDY OF PSR J1713+0747

RYAN M. SHANNON^{1,2} & JAMES. M. CORDES²*Draft version September 27, 2018*

ABSTRACT

Most millisecond pulsars, like essentially all other radio pulsars, show timing errors well in excess of what is expected from additive radiometer noise alone. We show that changes in amplitude, shape and pulse phase for the millisecond pulsar J1713+0747 cause this excess error. These changes appear to be uncorrelated from one pulse period to the next. The resulting time of arrival variations are correlated across a wide frequency range and are observed with different backend processors on different days, confirming that they are intrinsic in origin and not an instrumental effect or caused by strongly frequency dependent interstellar scattering. Centroids of single pulses show an rms phase variation $\approx 40 \mu\text{s}$, which dominates the timing error and is the same phase jitter phenomenon long known in slower spinning, canonical pulsars. We show that the amplitude modulations of single pulses are modestly correlated with their arrival time fluctuations. We also demonstrate that single-pulse variations are completely consistent with arrival time variations of pulse profiles obtained by integrating N pulses such that the arrival time error decreases proportional to $1/\sqrt{N}$. We investigate methods for correcting times of arrival for these pulse shape changes, including multi-component TOA fitting and principal component analysis. These techniques are not found to improve the timing precision of the observations. We conclude that when pulse shape changes dominate timing errors, the timing precision of PSR J1713+0747 can be only improved by averaging over a larger number of pulses.

Subject headings: gravitational waves, methods: statistical, pulsars: general, pulsars: specific (PSR J1713+0747)

1. INTRODUCTION

The timing of pulsars has enabled many studies of fundamental importance to physics and astrophysics, including precision tests of general relativity (Taylor & Weisberg 1982; Kramer et al. 2006), strong constraints on nuclear equations of state (Lattimer & Prakash 2007; Demorest et al. 2010), and the discovery of the first Earth-mass planets outside of the solar system (Wolszczan & Frail 1992). By studying the correlated variations in pulse times of arrival (TOAs) from a set of millisecond pulsars (MSPs) that comprise a pulsar timing array (PTA), it is possible to detect nanohertz gravitational waves (GWs) (Hellings & Downs 1983; Foster & Backer 1990). Candidate sources of GWs in the nanohertz frequency band are binary supermassive black holes in the throes of merger, oscillating cosmic strings, and the inflation era Universe (Jenet et al. 2009). The net perturbation due to these sources to TOAs is expected to be at most tens of nanoseconds over 5 – 10 years.

The most plausible source of gravitational waves is a stochastic background associated with massive black hole binaries (Jaffe & Backer 2003; Sesana et al. 2008). For

this background, a modestly significant ($\lesssim 4\sigma$) detection can be achieved by observing 20 to 40 pulsars over 5 to 10 years (Jenet et al. 2005) assuming monthly observations with 100 ns timing precision.

The required timing stability of $\lesssim 100$ ns can only be achieved with MSPs, pulsars with spin periods between ≈ 1 and 20 ms, which are more spin stable than canonical pulsars (CPs, pulsars with spin periods between ≈ 30 ms and 8 s). Over periods of years, CPs show large levels of correlated spin noise likely associated with instabilities in both the pulsar magnetosphere and the neutron star itself (Cordes & Downs 1985; D’Alessandro et al. 1995; Lyne et al. 2010; Shannon & Cordes 2010).

The precision of pulsar timing is at minimum limited by radiometer noise associated with the telescope receiving system and sky background. If this is the only form of noise, the sensitivity of observations is improved by increasing observation bandwidth, increasing observing time, or by increasing telescope sensitivity through larger collecting area or lower system temperature.

However, there are certainly other processes that affect the timing precision of pulsars and limit the sensitivity of PTAs to GWs. The sources and importance of a wide range of effects are summarized in Cordes & Shannon (2010). Stochastic timing variations can be broadly bifurcated into those with stationary statistics, such as white noise, and others that have or appear to have nonstationary statistics, such as those with very broad

ryan.shannon@csiro.au
cordes@astro.cornell.edu

¹ CSIRO Astronomy and Space Science, Box 76, Epping, NSW 1710, Australia

² Astronomy Department, Cornell University, Ithaca, NY 14853, USA

fluctuation spectra, including steep power laws with most of the power at low frequencies, often described as “red” processes. Red-like timing noise appears to describe the residuals seen in many canonical pulsars though it is still under debate whether on the longest times scale, the timing variations have non-stationary statistics or show band-limited or quasi-periodic statistics (Lyne et al. 2010; Shannon & Cordes 2010). Propagation of radio emission through the interstellar medium (Armstrong 1984; Coles et al. 2010; Cordes & Shannon 2010) also produces timing variations that have red power spectra.

On shorter time scales ranging from one pulse period to integrations from several minutes to an hour, TOA variations exceed what is expected from radiometer noise alone. In a study of CPs, Cordes & Downs (1985) demonstrated that timing errors were generally always larger than expected from additive radiometer noise and interpreted the excess in terms of changes in pulse shape and amplitude on pulse-to-pulse time scales. Termed “jitter,” this phenomenon has been seen in virtually all pulsars that have been closely investigated. Integrated pulse profiles include these variations and thus so do the TOAs derived from them.

While the link between single pulses and timing variations is well established in CPs, studies of MSPs are fewer because MSPs typically have much lower flux densities. However, a few cases indicate that single-pulse variations in MSPs are consistent with those seen in CPs. Jenet et al. (1998) studied the variability of single pulses of the bright millisecond pulsar J0437–4715. They found that single pulses contained a wide variety of morphologies and concluded the emission showed similar properties to that observed in canonical pulsars. Osłowski et al. (2011) followed up this analysis by identifying a correlation between arrival time and pulse shape changes, and used this correlation to improve timing precision by 20%. In a more recent study of PSR J0437–4715, Liu et al. (2012) found excess timing errors that they attributed to pulse shape variations. Edwards & Stappers (2003) analyzed the intensity modulation of a set of northern MSPs and suggested that there are periodic intensity modulations in MSP arrival times comparable to the drifting sub-pulse phenomenon observed in many canonical pulsars. Jenet & Gil (2004) found remarkable intensity stability of the main pulse of PSR B1937+21, but accompanied by large intensity modulation in giant pulse emission. Kramer et al. (1999) showed that the relative intensity of the components of the MSP J1022+1001 change on longer time scales and that a better timing solution for this pulsar could be obtained when these changes were incorporated.

In this paper, we focus on high S/N observations of the millisecond pulsar J1713+0747 to analyze fast pulse shape variations through measurements of single pulses and average pulse profiles. In Section 2, we summarize the observations and the data reduction procedure. In Section 3, we infer both directly and statistically that intrinsic pulse shape changes cause TOA variations in this pulsar. In Section 4, we rule out other processes that mimic pulse jitter in our observations. In Section 5, we present two different correction procedures that can

be used to correct for TOA variations and apply the techniques (unsuccessfully) to our observations. In Section 6, we discuss observing strategies that mitigate the effects of pulse profile variations on timing precision.

2. OBSERVATION AND ANALYSIS PROCEDURE

The relatively nearby MSP J1713+0747 has a period $P = 4.57$ ms, dispersion measure $DM = 16$ pc cm⁻³, and a pulse width of 110 μ s (FWHM) (Manchester et al. 2005). Its large (period averaged) flux density of 7.4 mJy at 1.4 GHz contributes to its being one of the best MSPs in terms of timing precision. We observed PSR J1713+0747 at 1.5 GHz with the Arecibo 305-m telescope³ using the “L-band Wide” receiver, which provides two channels, one for each hand of circular polarization. The results presented here use data recorded with two backend signal processing instruments: the Wide-band Arecibo Pulsar Processor (WAPPs, Dowd et al. 2000) and the Arecibo Signal Processor (ASP, Demorest 2007). The ASP backend is used for several long-term timing programs, including precision timing for GW detection. We use the WAPP data to study single-pulses but the ASP data to analyze TOA and pulse-shape variations of average profiles. The combination of data then allows us to connect single-pulse results to the long-term timing programs on PSR J1713+0747 that make use only of average profiles.

The WAPP data provided $\sim 50k$ pulses over a 4-minute time span on MJD 54983 and were used to analyze single pulses and sub-integrations of up to 512 pulses. Specifically, the WAPP instrument outputs a time series of autocorrelation functions (ACFs) of both polarizations with 3-level sampling. Offline, the `sigproc` package⁴ was used to Fourier transform the ACFs into spectra with 192 frequency channels across a 100 MHz total bandwidth spanning 1.57 to 1.67 GHz with 32 μ s resolution. After excising RFI, the data were dedispersed to form a single time series in the sum of the two polarization channels, which we call the total intensity. We used the `dspsr` software package (van Straten & Bailes 2011) to fold the data into subintegrations containing 1 to 1000 pulses, and the `psrchive` software package (Hotan et al. 2004) to measure TOAs from the subintegrations.

The ASP backend removes dispersion coherently to produce dedispersed time series in all four Stokes parameters which were then synchronously averaged in real time using the pulsar ephemeris. Averages were outputted every 10 s for 16 sub-bands, each with 4 MHz bandwidth, for a total of 64 MHz centered at 1410 MHz.

The `ASPFitsReader` pipeline was used to calibrate and generate TOAs (Ferdman 2008) from ASP measurements. Polarization calibration and absolute flux calibration were completed by comparing a pulsed signal generated by a noise diode while the telescope was pointed on and off a calibrating source to the pulsed signal while the telescope was pointed at the pulsar. The radio galaxy CTD 93 was used as the calibration source because it is

³ The Arecibo Observatory is part of the National Astronomy and Ionosphere Center, which was operated by Cornell University under a cooperative agreement with the National Science Foundation.

⁴ `sigproc.sourceforge.net`

known to be both unpolarized and to have no observed flux variability (Shaffer et al. 1999). For each channel, the receiver was calibrated for differential gain and phase offset between the feeds.

We calculated TOAs from both the WAPP and ASP data by using a matched-filter algorithm implemented in the Fourier domain (Taylor 1992). In this approach, TOAs are estimated by comparing the observed total intensity pulse profile $I(\phi)$ to a standard template $T(\phi)$. The matched-filtering approach is based on the assumption that the measured pulse profile is a scaled version of the template added to a measurement error term,

$$I(\phi) = aT(\phi - \phi_o) + b + n(\phi), \quad (1)$$

where a , b and ϕ_o are unknown parameters, and $n(\phi)$ is noise. Under the assumptions underlying Equation (1), the TOA uncertainty is $P\delta\phi_o$, where $\delta\phi_o$ is the standard error of ϕ_o .

For the ASP observations, templates for each observing band were generated from high-S/N observations of the pulsar co-added from the long-term Arecibo/NANOGrav⁵ timing program, which at present uses backend instrumentation and observing bands identical to those used in the work presented here (M. Gonzalez, private communication). For the WAPP observations, we produced an analytic template containing five Gaussian components, consistent with the average profiles in these observations, and comparable to a previous model of the profile described in Kramer et al. (1998).

Residual TOAs were then calculated by fitting a timing model ephemeris to the TOAs. For the observations here, we used an initial timing ephemeris derived from long term monitoring of J1713+0747 conducted at the Arecibo observatory (Demorest et al. 2012).

3. EVIDENCE FOR PULSE PHASE JITTER

3.1. Single Pulse Profile Variations

In this section, we examine single pulses from PSR J1713+0747. The 50k individual pulses obtained over four minutes allow pulse shape variations to be characterized during an interval when the modulation from diffractive interstellar scintillation (DISS) is approximately constant, since the characteristic DISS time scale is about one hour at 1.5 GHz.

The single pulse signal to noise ratio (S/N , defined as the ratio of peak intensity to the rms off-pulse intensity) ranged from approximately 1 to 30. In Figure 1, we show four relatively bright single pulses that have different morphologies with peak locations and pulse widths varying by amounts that cannot be attributed to radiometer noise.

Figure 2 shows average profiles that have been calculated using single pulses selected from different S/N ranges; each profile has been normalized to reflect the total detected flux in the S/N range. Despite occurring three times less frequently than the faintest pulses, the brightest and narrowest pulses contribute a total flux that is

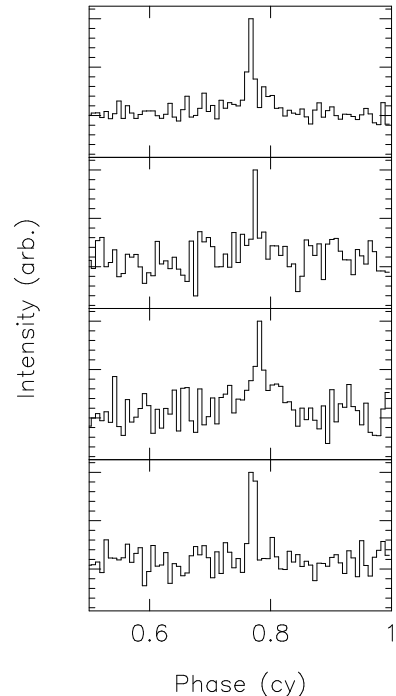


Figure 1. : Pulse intensity versus phase (measured in cycles, cy) for four single pulses from PSR J1713+0747. The pulses have been scaled to the same peak amplitude to show differences in shape and centroid pulse phase.

comparable to that of the faintest pulses. We also find that brighter pulses are narrower with peaks concentrated closer to the leading edge of the average pulse, suggesting that brighter pulses have earlier arrival times, which we will show below.

The presence of bright single pulses on the leading edge of the integrated pulse can be verified through a number of other diagnostics. One of these is the intensity modulation index, defined as

$$m_I(\phi) = \frac{\sqrt{\sigma_I^2(\phi) - \sigma_{I,\text{off}}^2}}{I(\phi)}, \quad (2)$$

where $I(\phi)$ and $\sigma_I(\phi)$ are the mean and rms intensity at phase ϕ and $\sigma_{I,\text{off}}$ is the rms off pulse intensity. The modulation index measures the normalized rms intensity across pulse phase ϕ and is sensitive to the frequency of occurrence of pulses at each pulse phase. A comparison of $m_I(\phi)$ with the integrated profile (Figure 3) indicates that the modulation index is largest at the leading edge of the pulse. This suggests the existence of a tail of bright pulses on the leading edge that has large enough amplitudes to dominate the modulation index.

The separations between strong pulses in units of the pulse period appear to be random. In Figure 4, we show the histogram for the spacing in arrival time ΔP for bright pulses with $S/N > 14$. The histogram of ΔP is fit well by an exponential distribution and is therefore consistent with a Poisson process. The mean spacing is ~ 150 pulses. The exponential distribution is the same as found for giant pulses from the Crab pulsar (Lundgren et al. 1995).

⁵ www.nanograv.org

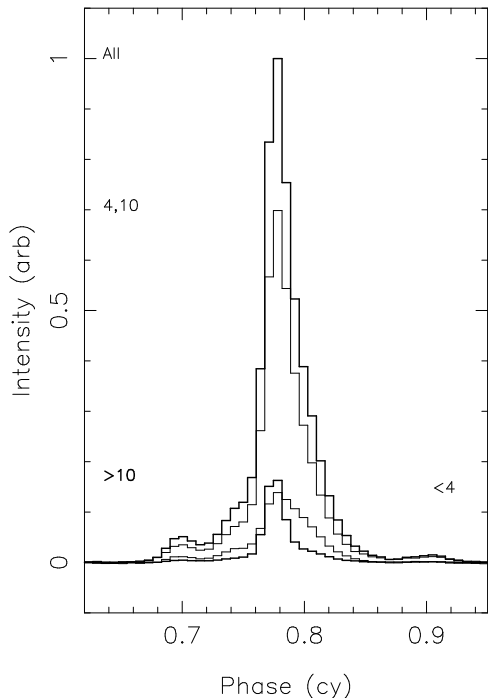


Figure 2. : Average pulse profiles for different ranges of S/N . The pulse profiles were formed from single pulses with S/N in the different ranges. The ranges are $S/N < 4$, $4 < S/N < 10$ (labeled on the plot as 4, 10), $S/N > 10$, and for all S/N ranges, and are labeled on the plot at a height close to the peak flux for each pulse profile, in a line thickness corresponding to the thickness of the pulse profile. The profiles are normalized to the total fluence so the profiles reflect the relative flux being emitted in these S/N ranges.

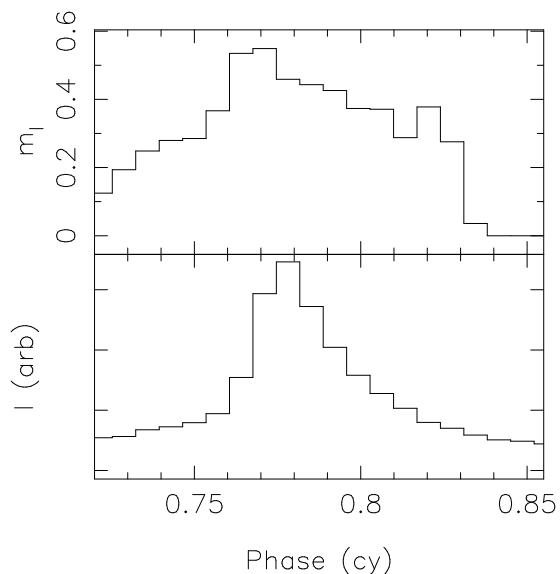


Figure 3. : Top panel: Modulation index m_I as a function of pulse phase ϕ calculated using equation (2). The leading edge of the pulse shows the largest m_I . Bottom panel: Average pulse profile.

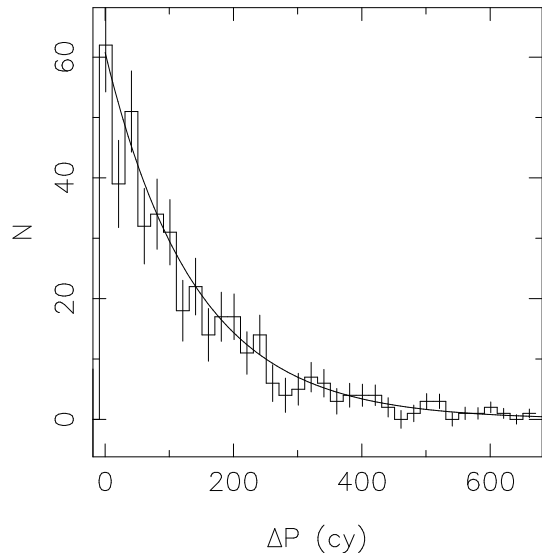


Figure 4. : Histogram of the spacing ΔP of bright pulses. The thin line shows the expected exponential distribution for ΔP if the number of bright pulses per unit time is Poisson distributed.

3.2. Single Pulse Timing

There is a modest correlation between single pulse S/N and pulse arrival time. In Figure 5, panel c, we show a scatter plot of residual arrival times Δt versus S/N for all pulses with $S/N > 3$. Brighter pulses tend to have earlier arrival times. In panels a and b, we display histograms of Δt for bright ($S/N > 20$) and weak ($14 < S/N < 20$) pulses, respectively. The weaker pulses arrive in a wide range of Δt , whereas the brightest pulses arrive in a narrower range of arrival time. While there is a clear correlation between arrival time and S/N , the correlation is not strong and the scatter in arrival times (labeled σ_J on the plot) is comparable in magnitude of the correlation. We note that a correlation between S/N and arrival time had previously been observed in the bright canonical pulsar PSR B0329+54 (McKinnon & Hankins 1993). This correlation was identified with mode changing and has a different character than the fast jitter effect observed in PSR J1713+0747.

In Figure 5, panel d, we show the histogram for S/N , which is a proxy for pulse intensity. For $S/N > 3.5$, the distribution is well described by a log-normal distribution. We fit a log-normal distribution to the histogram for $S/N > 3.5$ and found a reduced χ^2 of 1.7. This distribution is consistent with what is observed in canonical pulsars (Cairns et al. 2004). The distribution diverges from a log-normal distribution when $S/N \lesssim 3$ because radiometer noise (and not intrinsic brightness) dominate the estimate of pulse intensity. The distribution is highly inconsistent with a power-law distribution because the observed distribution does not show a long tail of pulses at high S/N . The best-fit power law produced poorly matched the data and had a reduced χ^2 of 150.

3.3. Timing Fluctuations for Integrated Profiles

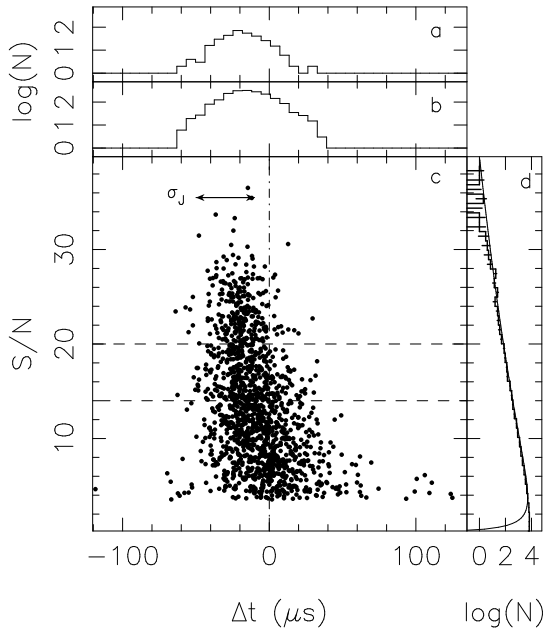


Figure 5. : Single pulse amplitude and arrival time statistics for PSR J1713+0747. Panel a: Histogram of the arrival times for very bright ($S/N > 20$) single pulses. Panel b: Histogram for weaker single pulses ($14 < S/N < 20$). Panel c: Scatter plot of residual arrival time Δt versus S/N for single pulses. The horizontal dashed lines indicate the S/N ranges used for panels a and b. The vertical dashed-dot line shows the mean pulse arrival time. For clarity, only a random selection of the single pulses have been plotted. To compensate for fewer bright single pulses, the probability of a pulse being selected was scaled $\propto 1/\rho(S/N_i)$, where $\rho(S/N)$ is the probability density function for S/N derived empirically from panel d. Panel d: Histogram of the S/N of single pulses. On the histogram, we also plot the 1σ counting errors. The best-fit curve to a log-normal distribution is displayed as a thin line.

Analysis of integrated pulse profiles produced by the ASP instrument confirms that intrinsic pulse shape variations are manifested as TOA variations in the integrated profiles.

In Figure 6, the residual TOAs for ASP observations are displayed for observations from MJD 54978, a day in which diffractive and refractive scintillation enhanced the flux in the 64 MHz ASP band by a factor of ≈ 4 . Within the figure, we show residual arrival times for simultaneous observations within three sub-bands of 4 MHz bandwidth, widely spaced across the band. The error bars represent the white noise uncertainty in the TOA estimates and vary in size between the sub-bands and in time because the flux (though relatively high in all bands) is modulated by diffractive scintillation.

Figure 6 also shows histograms of the residual TOAs for the three sub-bands. The values for skewness and kurtosis that we estimate indicate that the histograms are consistent with Gaussian distributions.

The arrival times are strongly correlated between the sub-bands. In Figure 7, we show a scatter plot of the residual arrival times in two frequency bands. A

best fit line to the data shows a slope consistent with unity, implying that the white-noise component of the TOA variations not caused by radiometer noise is essentially independent of frequency. This analysis was conducted for all pairs of frequency channels, and in all cases a slope consistent with unity was found. We note that a similar correlation between sub-banded TOAs was found in Parkes observations of PSR J0437–4715 by Osłowski et al. (2011), suggesting that the effect is not observatory dependent.

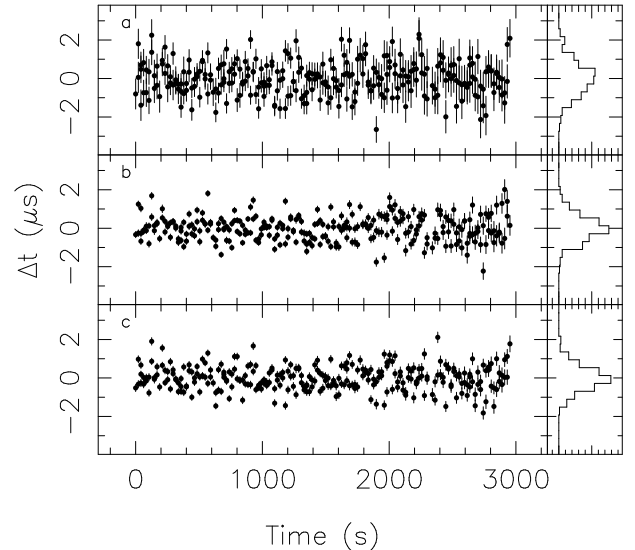


Figure 6. : Left panels: Residual TOAs for observations simultaneously obtained in three sub-bands of 4 MHz bandwidth. The central frequencies of the bands are 1382 MHz for panel a, 1410 MHz for panel b, and 1430 MHz for panel c. Right panel: Histograms of residual TOAs.

Another demonstration of the large correlation of the TOA variations across frequency is given in Figure 8, which shows the cross correlation functions (CCFs) for arrival time variations between the three pairs of sub-bands. The CCFs show spikes at zero lag that drop to zero correlation after one sample (10 s). The zero-lag spike confirms that the residual TOAs are correlated between different frequency channels, and that the structure is unresolved in time at the 10 s level. This is consistent with what would be expected if the single pulse modulation affecting the WAPP observations was causing the timing error observed in the ASP observations, because the variations appear to be uncorrelated with time.

If we define the rms pulse-phase jitter σ_J as the excess white-noise residual over that expected from radiometer noise, we can estimate it from the CCF because radiometer noise will not correlate between different frequency bands while the jitter will. The zero-lag value is $\text{CCF}(0) = \sigma_J^2 \approx 0.30 \mu\text{s}^2$, so $\sigma_J \approx 0.55 \mu\text{s}$ for $T = 10$ s (2188 pulses). This corresponds to jitter in single-pulse arrival times of $\sqrt{2188} \times 0.55 \mu\text{s} \approx 26 \mu\text{s}$, compared to the pulse width (FWHM) of $110 \mu\text{s}$. Our observation of shape variations are consistent with a model presented

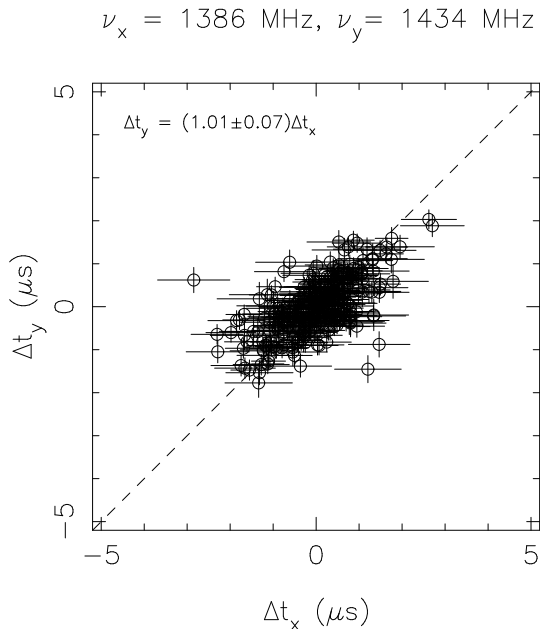


Figure 7. : Correlation of TOAs between two frequency channels. The error bars represent the $1 - \sigma$ template fitting errors. The dashed angled line indicates $\Delta t_y = \Delta t_x$.

in Cordes & Downs (1985), in which single pulses are modeled to have narrower profiles than the mean profile, but large variations in centroid. Shape variations can then be characterized by a dimensionless jitter parameter $f_J = 1 - (w_i/w_a)^2$, where w_i is the width of a single pulse and w_a is the width of an average pulse. For PSR J1713+0747, we find a jitter parameter $f_J \approx 0.24$, which is consistent with values found for other pulsars (Cordes & Downs 1985).

3.4. Connecting Single Pulse Timing Variations to Standard Precision Timing Observations

Phenomenologically, it has been known since the early days of pulsar timing that despite the phase jitter of individual pulses, integrated profiles converge toward an average shape that is stable on time scales of decades. This convergence corresponds to timing precision that improves as $1/\sqrt{N_p}$ when N_p pulses are summed (Helfand et al. 1975). For some long-period pulsars, the effective number of independent pulses is less than N_p because there are short term correlations and the results for J1713+0747 are consistent with a lack of correlations.

We demonstrate that the arrival-time errors from standard template fitting to average profiles obtained by averaging $N_p \gg 1$ pulses are completely consistent with the directly measured pulse-to-pulse variations. We do so by comparing the actual timing errors from ASP data with the errors expected under idealized conditions where an average profile is the sum of the template and additive white noise. In the top panel of Figure 9, the rms residual $\sigma(N_p)$ is plotted against the number of pulses averaged, N_p , for both ASP and WAPP observations (open symbols). We also show rms timing residuals $\sigma_r(N_p)$ ex-

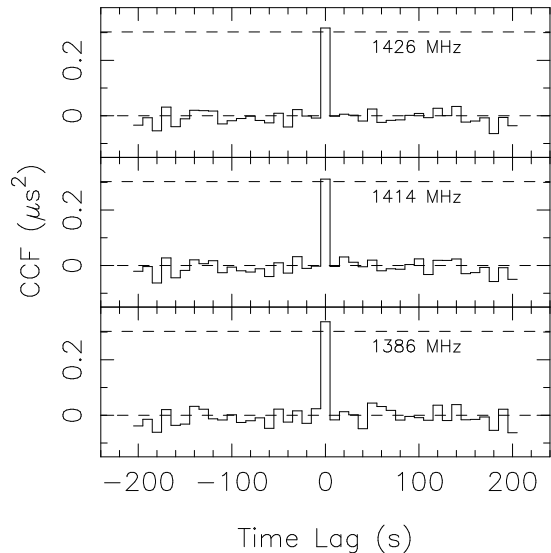


Figure 8. : Cross correlation function between time series for the 1430 MHz channel and three other channels. The lower dashed lines show the zero correlation level. The CCF shows a spike at zero lag that decays to zero in one sample (10 s). The upper dashed lines show the level of jitter inferred from Figure 9.

pected if there were only additive radiometer noise and no phase jitter (filled symbols). Values for σ_r were estimated from simulated pulse profiles calculated by adding white noise to the template shape using the S/N appropriate for the data. The simulated profiles were analyzed identically to the observations to produce arrival time estimates. These simulated profiles also satisfy the conditions for matched filtering and therefore yield the smallest possible timing error under the assumption that there is minimally stationary (white) noise present in the timing observations (Turin 1960). The predicted rms error for additive noise alone is much less than σ . Both σ and σ_r decrease proportionally to $1/\sqrt{N_p}$, as expected for timing errors that are uncorrelated between pulses.

In the bottom panel of Figure 9, we show the quadrature difference between the actual and predicted timing errors

$$\sigma_J(N_p) = \sqrt{\sigma^2(N_p) - \sigma_r^2(N_p)}. \quad (3)$$

After accounting for the different numbers of pulses averaged, the values of σ_J obtained from the WAPP and ASP observations consistent with each other. The single-pulse value $\sigma_J(1) \approx 27 \pm 1 \mu\text{s}$ is consistent with the value derived from the cross-correlation analysis in the previous section. The total timing error is a combination of both phase jitter and radiometer noise.

4. CONFIRMING THE JITTER HYPOTHESIS

We have shown that the excess timing error is broadband and uncorrelated between pulse profiles calculated from disjoint sets of pulses. In addition to jitter, there are two other plausible forms of timing error that can contribute errors of this nature: diffractive interstellar scintillation and observation calibration. Here we rule out both of these alternative explanations.

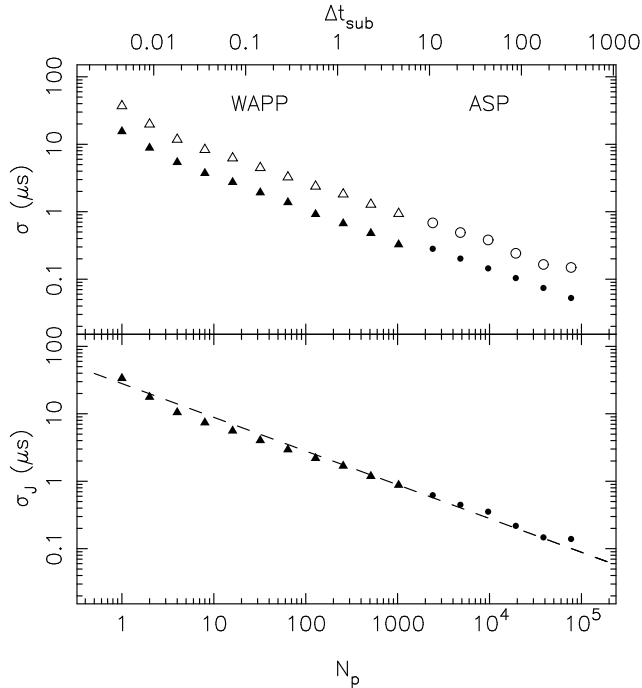


Figure 9. : Top panel: Measured rms (unfilled symbols) and expected rms (filled symbols) timing residuals versus the number of pulses averaged N_p , for observations using the WAPP (triangles) and ASP backends (circles). Bottom panel: Quadrature difference between observed and expected rms timing errors. The dashed line is a fit to the data, showing the expected scaling $\sigma_J(N_p) \propto N_p^{-1/2}$. Despite having different levels of radiometer noise, the level of jitter extrapolated from the WAPP observations is consistent with the ASP observations. The horizontal scale at the top of the plot gives the integration time in seconds of sub-integrations Δt_{sub} corresponding to N_p in the bottom scale.

Diffraction interstellar scintillation (DISS) will generally modulate the pulse shape on minutes to hour time scales, depending on observing frequency, dispersion measure, and direction. The shape perturbation is uncorrelated over a time equal to the diffractive time scale t_d and over a frequency range equal to the scintillation bandwidth, ν_d (Cordes et al. 1990; Hemberger & Stinebring 2008; Cordes & Shannon 2010). The DISS time scale and bandwidth vary strongly with observing frequency, approximately as ν^{-1} and ν^{-4} , respectively. The DISS timing perturbation has been observed in another (but much more strongly scattered) MSP, PSR B1937+21 (Cordes et al. 1990; Jenet & Gil 2004).

DISS is ruled out as the source of the excess TOA variation observed for MSP J1713+0747. First, diffractive TOA variations would be correlated over a time comparable to the 1 hr diffractive time scale whereas the TOA variations appear to vary on a time scale shorter than the rotation period of the pulsar (4.6 ms). Also, the timing perturbation expected from DISS is much smaller than the observed timing error. Diffractive scintillation is expected to contribute an rms error of (Cordes et al. 1990;

Coles et al. 2010; Cordes & Shannon 2010)

$$\Delta t_{\text{DISS}} \approx \tau / \sqrt{N_s}. \quad (4)$$

where τ is the pulse broadening time and N_s is the number of “scintles,” which are the number of bright patches of constructive interference contained in the frequency-time plane of an observation. The number of scintles is $N_s \approx (1 + 0.3T/t_d)(1 + 0.3\Delta\nu/\Delta\nu_d)$ (Cordes et al. 1990), where T is the observing time for each sub-integration (which for our observations vary in duration between the rotation period of a pulsar 4.6 ms and $\approx 10^2$ s), t_d is the diffractive time scale (> 1 hr), $\Delta\nu$ is the observing bandwidth 100 MHz and $\Delta\nu_d$ is the diffractive scintillation bandwidth (≈ 50 MHz). Thus for the observations reported here, $N_s \approx 1$. The pulse broadening time can be inferred from the scintillation bandwidth $\tau = C_1/2\pi\Delta\nu_d$, where $\Delta\nu_d$ is the scintillation bandwidth and C_1 is a constant of order unity (Cordes & Rickett 1998). Evaluating Equation (4), we find that $\Delta t_{\text{DISS}} \approx 3$ ns, which is much less than the rms scatter of 26 μs .

It is also possible that instrumental effects (including both calibration errors and radio frequency interference) can cause pulse shape changes. However we disfavor this origin. We convincingly connect the levels of jitter observed in ASP observations with that observed in WAPP observations. These backends operate with different architectures. They also have different sampling levels, suggesting that artifacts of digitization, such as scattered power (Kouwenhoven & Voûte 2001), are not grossly affecting the 3-level sampled WAPP observations. The jitter is observed at modestly different frequencies (ruling out narrow-band RFI). In a previous observing campaign in which PSR J1713+0747 was observed simultaneously with the Arecibo and Green Bank telescopes, residual TOAs were found to be correlated on similarly short time scales at the same observing frequency (Lam & Demorest 2010). Calibration errors associated with non-orthogonality of the feeds should be uncorrelated between the different telescope feeds. Additionally, timing errors induced will change slowly as the orientation of the feed with respect to the pulsar changes. Radio frequency interference (RFI) could also plausibly cause timing error. Interference is local to each telescope and will be uncorrelated between telescopes separated by thousands of kilometers.

The correlation between larger S/N and earlier arrival times is seen only at the single-pulse level and is therefore only observed in the WAPP data sets. Our interpretation is that the effect is evidently diminished in averages of 10 s or longer. There is no evidence that the correlation is caused by instrumental effects. Firstly, the effects of digitization are small because the signal to noise ratio of the detected, non-dispersed signal is low. The dispersion smearing across the band is approximately 3 ms (much greater than the pulse width) so the non-dispersed signal has an S/N of approximately 0.7. Distortions in pulse shapes are strongest when the dispersive delay across the band is comparable to the pulse width and are suppressed when the delay is much larger than the pulse width (Stairs et al. 2000). The dominant effect of digitization is the appearance of negative detected power (dips) at the edges of the pulse profile (Jenet & Anderson

1998). We see no evidence for this type of distortion in our data. For example in Figure 2, the baseline is flat at the edge of even the brightest pulses ($S/N > 10$) that would be the most affected by distortions. The most convincing demonstration of an intrinsic origin for the correlation between S/N and arrival time would be to observe the same effect with different instrumentation that provides fast-sampled data having more bits of representation (e.g., ≥ 8 bits) and preferably different architecture (e.g., a baseband recorder or a polyphase filterbank).

5. CORRECTING TOAS FOR PULSE SHAPE CHANGES

We investigated two distinct methods for correcting arrival times due to short term variations: multi-component template fitting and principal component analysis (PCA). These techniques were tested on both ASP and WAPP data, enabling us to test the correction algorithms on data over a wide range of pulse averaging. We were unable to develop an algorithm to improve the precision of arrival times using pulse shape information. We attribute the lack of success to the absence of a sufficiently strong correlation between pulse shape changes and arrival times presented in the previous sections. Here we briefly summarize two attempts at correction and defer further discussion to a future paper.

We implemented a multi-component TOA fitting algorithm similar to one that was used to improve the timing precision of PSR J1022+1001 (Kramer et al. 1999). For PSR J1713+0747, we constructed an analytic template containing 5 Gaussian components, consistent with previous models of the pulsar (Kramer et al. 1998). We then made a non-linear fit for the shape parameters, i.e., the amplitude, widths, and relative positions of the different components. The TOAs generated with this technique were then compared to TOAs inferred using the standard method. We found no improvement in the residual arrival times from TOAs derived from the non-linear technique.

We also conducted principal component analysis (PCA) on our data using a method comparable to one presented in Osłowski et al. (2011), though implemented using a different algorithm.

To briefly summarize our algorithm, we calculated data vectors by subtracting the average pulse profile from individual profiles. The covariance matrix of the data vectors was then diagonalized to obtain the eigenvalues and eigenvectors.

A scalar quantity, formed by projecting the observed pulse profiles onto the most significant eigenvectors, is then calculated and correlated with the residual TOAs. Any significant correlation between the scalar and residual TOAs indicates that a particular eigenvector contains aspects of profile variation that is influencing arrival times. Osłowski et al. (2011) found such an eigenvector for PSR J0437–4715 and were able to use the correlation to improve the timing precision of the pulsar. For PSR J1713+0747, we found no significant correlation between any eigenvector and residual arrival time and were therefore unable to implement any correction technique using TOAs.

For both PSR J1022+1001 and PSR J0437–4715, cor-

related pulse shape changes are highly significant in integrated pulse profiles, with sub-integrations separated by minutes to days showing differences in pulse shape visible by eye. For PSR J1713+0747, the pulse shape changes appear to decorrelate on pulse to pulse time scales on the millisecond-hour baselines probed by the observations presented here.

6. DISCUSSION AND CONCLUSIONS

We have demonstrated that pulse jitter is the dominant source of timing error in the observations of PSR J1713+0747 presented here. This pulsar is currently being monitored by the three major pulsar timing array collaborations: the European Pulsar Timing Array (EPTA, Ferdman et al. 2010), the North American Nanohertz Observatory for Gravitational Waves (NANOGrav, Jenet et al. 2009), and the Parkes Pulsar Timing Array (PPTA, Verbiest et al. 2010). Based on the observations presented here, the timing error induced by shape variations can be extrapolated to the longer observing spans typically used in pulsar timing array observations. For a 30 min observation with $N_p \approx 10^{5.6}$, we predict $\sigma_J \approx 40$ ns. This is consistent with the rms error observed in the long term timing precision of this object (Demorest et al. 2012), suggesting that a significant component of the timing error is associated with jitter.

Pulse shape changes, if uncorrelated on time scales longer than typical observing cadences and uncorrectable using information about pulse shape changes, contribute additional white noise to TOAs. In general there are three avenues for reducing white noise in timing observations: observing with a more sensitive telescopes, observing with a wider observing bandwidth, or averaging over a larger number of pulses. Of these three options, only the last can be used to reduce timing error associated with jitter because the TOA perturbations are broadband and independent of antenna gain. This implies that many pulsars may need to be observed with higher throughput (i.e. with longer observations at each epoch, or observed with shorter cadence) to make a convincing detection of the gravitational wave background (Cordes & Shannon 2012).

The timing precision of PSR J1713+0747 and probably other *bright* MSPs is likely limited by jitter if observed with telescopes where the single pulse $S/N \gtrsim 1$. If we assume that the pulse is Gaussian shaped with width w the rms associated with jitter is (Cordes & Downs 1985; Cordes & Shannon 2010)

$$\Delta t_J \approx w_i f_J (1 + m_I^2) N^{-1/2}, \quad (5)$$

where w_i is the intrinsic pulse width, f_J is the jitter parameter, m_I is the modulation index, and N is the number of pulses used to form each subintegration. In contrast, the rms expected from radiometer noise is

$$\Delta t_R \approx \frac{w_a}{S_0 \sqrt{N}} \quad (6)$$

where w_a is the width of the integrated pulse and S_0 is the single pulse S/N . We can solve for the critical S_0 by equating equations (5) and (6). We find that the

threshold single pulse signal to noise ratio is

$$\begin{aligned}
 S_c &\approx \frac{w_a}{w_i f_J (1 + m_J^2)} \\
 &\approx \frac{1}{f_J (1 - f_J)^{1/2} (1 + m_J^2)} \\
 &\approx 1.4 \left(\frac{1 - f_J}{0.5} \right)^{-1/2} \left(\frac{f_J}{0.5} \right)^{-1} \left(\frac{1 + m_J^2}{2} \right)^{-1}.
 \end{aligned} \tag{7}$$

The exact value of the transition depends on the magnitude of phase jitter, the modulation index, and the shape of the pulse. However we expect that for most pulsars the critical single pulse S/N will be close to unity.

Large telescopes provide other avenues for improving TOA precision. First, higher S/N observations will be able to better diagnose the pulse shape changes in a larger number of MSPs. Additionally, larger interferometric telescopes such as the SKA can provide a higher timing throughput if they possess the ability to form multiple sub-arrays. In this case, multiple pulsars can be observed simultaneously, with the gain of each sub-array tailored to individual pulsars.

Timing errors associated with shape changes are correctable only if they are accompanied by gross changes in the shape of the pulse. If not, correction is likely minimal because other astrophysical effects will cause similar displacement of the pulses (albeit on longer time scales). Though unsuccessful in the analysis of J1713+0747, multi-component template fitting and PCA are sensitive to subtle changes in the shape of pulses.

It is imperative to assess profile stability in all current and candidate MSPs for pulsar timing arrays. As we have demonstrated, single pulse measurements are not required to determine the amount of pulse phase jitter. It can readily be inferred from integrated profiles.

We thank the referee for suggestions that improved the quality of this paper. We thank G. Hobbs, S. Osłowski, and W. van Straten for useful discussions; and P. Freire, A. Venkataraman, and in particular T. Ghosh for assistance with the observations. RMS gratefully acknowledges NAIC for travel support for conducting the observations used in this analysis. This work was supported at Cornell University by the National Science Foundation through grant AST 0807151 and as a subaward from West Virginia University from NSF/PIRE Grant 0968296.

REFERENCES

- Armstrong, J. W. 1984, *Nature*, 307, 527
 Cairns, I. H., Johnston, S., & Das, P. 2004, *MNRAS*, 353, 270
 Coles, W. A., Rickett, B. J., Gao, J. J., Hobbs, G., & Verbiest, J. P. W. 2010, *ApJ*, 717, 1206
 Cordes, J. M., & Downs, G. S. 1985, *ApJS*, 59, 343
 Cordes, J. M., & Rickett, B. J. 1998, *ApJ*, 507, 846
 Cordes, J. M., & Shannon, R. M. 2010, arXiv:1010.3785
 —. 2012, *ApJ*, 750, 89
 Cordes, J. M., Wolszczan, A., Dewey, R. J., Blaskiewicz, M., & Stinebring, D. R. 1990, *ApJ*, 349, 245
 D’Alessandro, F., McCulloch, P. M., Hamilton, P. A., & Deshpande, A. A. 1995, *MNRAS*, 277, 1033
 Demorest, P. B. 2007, PhD thesis, University of California, Berkeley
 Demorest, P. B., Pennucci, T., Ransom, S. M., Roberts, M. S. E., & Hessels, J. W. T. 2010, *Nature*, 467, 1081
 Demorest, P. B., et al. 2012, ArXiv e-prints
 Dowd, A., Sisk, W., & Hagen, J. 2000, in *Astronomical Society of the Pacific Conference Series*, Vol. 202, IAU Colloq. 177: Pulsar Astronomy - 2000 and Beyond, ed. M. Kramer, N. Wex, & R. Wielebinski, 275
 Edwards, R. T., & Stappers, B. W. 2003, *A&A*, 407, 273
 Ferdman, R. 2008, PhD thesis, University of British Columbia
 Ferdman, R. D., et al. 2010, *Classical and Quantum Gravity*, 27, 084014
 Foster, R. S., & Backer, D. C. 1990, *ApJ*, 361, 300
 Helfand, D. J., Manchester, R. N., & Taylor, J. H. 1975, *ApJ*, 198, 661
 Hellings, R. W., & Downs, G. S. 1983, *ApJ*, 265, L39
 Hemberger, D., & Stinebring, D. R. 2008, *ApJ*, 674, L37
 Hotan, A. W., van Straten, W., & Manchester, R. N. 2004, *PASA*, 21, 302
 Jaffe, A. H., & Backer, D. C. 2003, *ApJ*, 583, 616
 Jenet, F. A., & Anderson, S. B. 1998, *PASP*, 110, 1467
 Jenet, F. A., Anderson, S. B., Kaspi, V. M., Prince, T. A., & Unwin, S. C. 1998, *ApJ*, 498, 365
 Jenet, F. A., & Gil, J. 2004, *ApJ*, 602, L89
 Jenet, F. A., Hobbs, G. B., Lee, K. J., & Manchester, R. N. 2005, *ApJ*, 625, L123
 Jenet, F. A., et al. 2009, astro-ph/0909.1058
 Kouwenhoven, M. L. A., & Voûte, J. L. L. 2001, *A&A*, 378, 700
 Kramer, M., Xilouris, K. M., Lorimer, D. R., Doroshenko, O., Jessner, A., Wielebinski, R., Wolszczan, A., & Camilo, F. 1998, *ApJ*, 501, 270
 Kramer, M., et al. 1999, *ApJ*, 520, 324
 —. 2006, *Science*, 314, 97
 Lam, M., & Demorest, P. 2010, *BAAS*
 Lattimer, J. M., & Prakash, M. 2007, *Phys. Rep.*, 442, 109
 Liu, K., Keane, E. F., Lee, K. J., Kramer, M., Cordes, J. M., & Purver, M. B. 2012, *MNRAS*, 420, 361
 Lundgren, S. C., Cordes, J. M., Ulmer, M., Matz, S. M., Lomatch, S., Foster, R. S., & Hankins, T. 1995, *ApJ*, 453, 433
 Lyne, A., Hobbs, G., Kramer, M., Stairs, I., & Stappers, B. 2010, *Science*, 329, 408
 Manchester, R. N., Hobbs, G. B., Teoh, A., & Hobbs, M. 2005, *AJ*, 129, 1993
 McKinnon, M. M., & Hankins, T. H. 1993, *A&A*, 269, 325
 Osłowski, S., van Straten, W., Hobbs, G., Bailes, M., & Demorest, P. 2011, arXiv:1108.0812
 Sesana, A., Vecchio, A., & Colacino, C. N. 2008, *MNRAS*, 390, 192
 Shaffer, D. B., Kellermann, K. I., & Cornwell, T. J. 1999, *ApJ*, 515, 558
 Shannon, R. M., & Cordes, J. M. 2010, *ApJ*, 725, 1607
 Stairs, I. H., Splaver, E. M., Thorsett, S. E., Nice, D. J., & Taylor, J. H. 2000, *MNRAS*, 314, 459
 Taylor, J. H. 1992, *Royal Society of London Philosophical Transactions Series A*, 341, 117
 Taylor, J. H., & Weisberg, J. M. 1982, *ApJ*, 253, 908
 Turin, G. 1960, *Information Theory*, *IRE Transactions on*, 6, 311
 van Straten, W., & Bailes, M. 2011, *PASA*, 28, 1
 Verbiest, J. P. W., et al. 2010, *Classical and Quantum Gravity*, 27, 084015
 Wolszczan, A., & Frail, D. A. 1992, *Nature*, 355, 145